A&A 385, 921–931 (2002)
DOI: 10.1051/0004-6361:20020161

Astronomy & Astrophysics

δ Scuti stars in Praesepe

II. The STACC 1998 campaign – The spectroscopy

T. H. Dall[1,2], S. Frandsen[1], H. Lehmann[3], G. C. Anupama[4], E. Kambe[5,⋆], G. Handler[6,⋆⋆], S. Kawanomoto[7], E. Watanabe[8], M. Fukata[5], T. Nagae[9], and S. Horner[10]

[1] Institute for Physics and Astronomy, University of Aarhus, Universitetsparken, Bygn. 520, 8000 Aarhus C, Denmark
[2] Nordic Optical Telescope, Apartado 474, 38700 Santa Cruz de La Palma, Spain
[3] Thüringer Landessternwarte, 07778 Tautenburg, Germany
[4] Indian Institute of Astrophysics, Koramangala, Bangalore 560 034, India
[5] Department of Geoscience, National Defence Academy, Yokosuka, Kanagawa 239-8686, Japan
[6] Institute for Astronomy, University of Vienna, Türkenschanzstrasse 17, 1180 Wien, Austria
[7] National Astronomical Observatory, 2-21-1 Osawa, Mitaka, Tokyo 181-8588, Japan
[8] Okayama Astrophysical Observatory, National Astronomical Observatory, Kamogata, Okayama 719-0232, Japan
[9] Department of Earth and Planetary Sciences, Kobe University, Kobe, Japan
[10] Lockheed Martin, 3251 Hannover St. L3-29 B201, Palo Alto, CA94304, USA

Received 29 May 2001 / Accepted 28 January 2002

Abstract. We present the results of a large international spectroscopic campaign on the δ Scuti star BN Cnc. Combining observations from five observatories taken over more than two weeks, we calculate line indices of the Hα line. A line index is the integrated line flux in a software filter divided by the continuum flux. We demonstrate that this can be used in combination with simultaneous photometry to classify the oscillation modes. We recover all the frequencies also found from photometry and assign likely mode identifications, which differ slightly from previously published values, but are found to be consistent with simple models. The difference in identification is found to have very little effect on the derived luminosity and temperature.

Key words. stars: oscillations – stars: variables: δ Scuti – open clusters and associations: individual: Praesepe – stars: individual: BN Cnc

1. Introduction

Among the most promising targets for successful application of asteroseismology are the δ Scuti stars. They have rich sets of oscillation modes which in many cases are readily observable. Unfortunately, each δ Scuti star is only found to oscillate in a seemingly random subset of possible modes, making it difficult to identify exactly which modes are observed. To further complicate matters, these stars tend to be rapid rotators, which causes displacement of the frequencies.

One approach to the problem is to observe a number of stars in a cluster sharing basic parameters like distance, metallicity and age in order to restrict the degrees of freedom in the model calculations. The Praesepe open cluster contains at least 14 δ Scuti stars, many of which have been the targets of a number of observing campaigns.

The stars BN Cnc and BV Cnc have both been studied extensively. The variability of BV Cnc was firmly established by Arentoft et al. (1998), who also found that BN Cnc has at least eight pulsation modes. The two stars are located only 2.52′ apart, which makes them excellent targets for differential CCD photometry.

The STACC network organised an international multi-site campaign in the first half of 1998 on BV Cnc and BN Cnc (Frandsen et al. 2001, hereafter Paper I). The aim of this campaign was, with a very long time-base of ∼3 months to provide accurate frequencies of the oscillation modes in these stars. During a few weeks in February 1998, BN Cnc (A7V, $V = 7.8$, $v \sin i = 115$ km s^{-1}) was also the target of a spectroscopic campaign aimed at providing enough information to be able to get a preliminary classification of the pulsation modes in this star using

Send offprint requests to: T. H. Dall, e-mail: tdall@ifa.au.dk
⋆ Visiting Astronomer, Okayama Astrophysical Observatory.
⋆⋆ Current address: South African Astronomical Observatory, PO Box 9, Observatory, 7935, South Africa.

line-indices of spectral lines. This paper deals with the results of the spectroscopic campaign on BN Cnc. See Paper I for the results of the photometric campaign.

The technique is described in Sect. 2, after a short overview of the spectroscopic techniques used for observing δ Scuti stars. The observations from all sites are presented in Sect. 3, the data reduction in Sect. 4, and the combination of all data is presented in Sect. 5. In Sect. 6 the frequency content and the amplitudes are derived, and Sect. 7 discusses the implications and attempts to identify the pulsation modes. Some concluding remarks are given in Sect. 8.

2. The mode identification problem

The past years have shown considerable effort to establish reliable mode identifications for a number of δ Scuti stars, but in most cases we are left with some ambiguity. Purely photometric techniques have the advantage of greater efficiency, and ultimately the ability to observe fainter stars than is possible with spectroscopy. A secure mode identification seems only possible, when several techniques agree. Especially for rotating stars, there are too many free parameters that one method can give a unique answer.

The photometric modal discrimination relies on model atmosphere calculations (e.g. Garrido 2000), which suffer from our lack of understanding of the physical conditions in δ Scuti stars. The "regions of interest" used in the photometric discrimination are not only partially overlapping, but also strongly dependent on model parameters.

Another method has been the calculation of thousands of models to try to reproduce the frequencies (e.g. Pamyatnykh et al. 1998 for the case of XX Pyx), but without any convincing results. In fact, no stellar model has yet provided a unique fit to any set of observed frequencies.

The detection of line-profile variations caused by non-radial pulsation modes has been made possible by detailed spectroscopic studies. High resolution spectroscopy combined with high time resolution provides the ultimate information and works for low as well as high degree modes. In this case, large telescopes with efficient spectrographs are needed. For a recent review consult Mantegazza (2000). A different approach is the moment method introduced by Balona and discussed by Aerts & Eyer (2000) where references are given. Both methods work well when there are only a small number of modes (i.e. for a star like ρ Pup with one radial mode), but when trying to fit a number of closely spaced modes, these spectroscopic methods are less powerful and often leave a lot of ambiguity in the classification. None of them has ever been applied to δ Scuti stars as faint as BN Cnc.

Detailed studies of line profile variations have been carried out for β Cephei stars (e.g. Telting & Schrijvers 1997 or Schrijvers et al. 1997). If the S/N of the spectra is sufficiently high, good indications of the mode type can be derived. This type of analysis is more difficult for δ Scuti stars, where the Doppler velocities are smaller.

A more efficient technique in terms of photon efficiency, which can work with a modest resolution spectrum, is the use of ratios between the amplitude of the variation of the equivalent width (EW) of the Balmer lines divided by a photometric amplitude (e.g. Dall 1998; Frandsen 2000). The EW can be measured with "FOSC" (Faint Object Spectroscopic Camera) type instruments which are very efficient (>20%) and easy to use. One can replace the EW by line-indices which rely on the temperature sensitivity and spatial sensitivity of the equivalent widths of spectral lines. It is a promising new technique, which has been successfully applied to a number of pulsating stars of different classes; the δ Scuti star FG Vir (Viskum et al. 1997, 1998), the roAp star α Cir (Baldry et al. 1998, 1999) and the EC14026 star PG1605+072 (O'Toole et al. 2000). It was suggested as a way to observe oscillations in solar-type stars by Bedding & Kjeldsen (1996) and has been theoretically explored for early type stars by Balona (2000). The variation of the EW basically tracks the changes in temperature and gravity. In δ Scuti stars the temperature dominates, while in EC14026 stars the gravity changes contribute at a similar level.

The modest resolution of the "FOSC" type instruments and the instrumental flexures caused by the mounting in the Cassegrain focus means that radial velocity measurements are difficult. This is the reason that radial velocities are not discussed in the present project, as the data from the other sites alone is not enough to derive a decent power spectrum of the radial velocity variations.

2.1. The line-indices

For calculating line-indices, the spectra do not need to be wavelength or continuum calibrated and thus consist of "counts per pixel" instead of fluxes as function of wavelength:

$$F_\lambda \longrightarrow S_x. \tag{1}$$

The quantity x is a pixel number and the unit of S is counts. One can of course work with fully calibrated spectra without problems.

The general idea is to integrate the counts in the line, using a suitable weight function, $W_x^{\rm L}$, which we will call a *filter-function* or just *filter*. A broad filter $W_x^{\rm C}$ is used for the continuum.

First the centre of the line is defined by moving an integration weight filter across the line, and choosing the point of maximum total counts as the line centre. The line centre is thus the position that maximises the counts in the filter, see Fig. 1.

With the line centre pinned the continuum C_x is calculated from two adjacent areas on each side of the line, which appears to have a well defined continuum between weak lines. This is done by rejection iterations, fitting a straight line to the continuum. Even if the continuum is not well defined e.g. because of a continuous blend of weak lines, it is still possible to obtain a continuum measure from this blend, only will this give a lower value for the

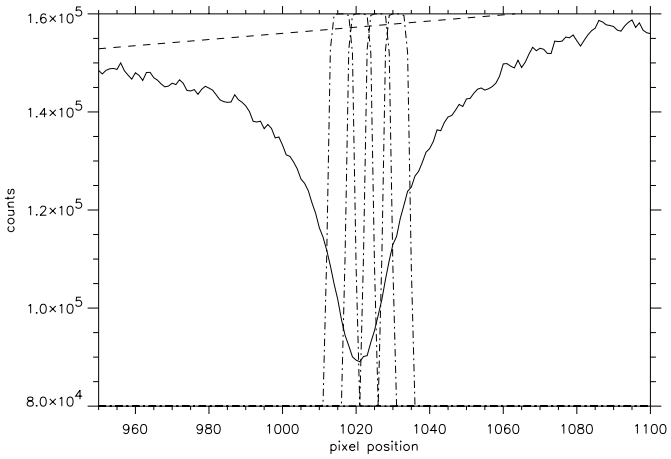

Fig. 1. To find the line centre a filter is moved across the line and the position that maximises the sum is the line centre. The width of the filter can be chosen arbitrarily. The dashed line is the fit to the continuum.

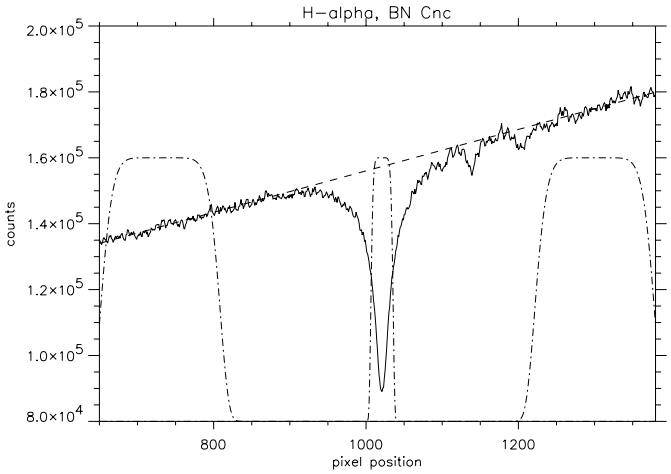

Fig. 2. An example of calculation of a line-index of Hα. The continuum is found from the two broad filters on each side, while the line-index is calculated as the counts in the line weighted by the central filter. Continuum slope and slow curvature do not pose a problem.

continuum. The effect will be to diminish each value of the line index by the same amount, which will in turn tend to make the apparent oscillation amplitude insignificantly larger.

With the chosen filter function $W_x^{\rm L}$ for the line in question, the integration is carried out across the line, yielding the line-index;

$$\Lambda^{\rm L} = \sum \frac{C_x - S_x}{C_x} W_x^{\rm L}. \quad (2)$$

The filter $W_x^{\rm L}$ typically fades off to zero as the line wings approach the continuum. An example of the weights used for continuum and line-index is given in Fig. 2. Thus, a line-index in a given filter will be proportional to the equivalent width (EW) of the line. It differs from a EW measurement in that it does not necessarily count the total flux in the line. In this sense it resembles the Strömgren Hβ index, just performed with software filters. The advantage is of course that any type and number of filters can be applied to any line in the data set.

The justification of the term "line index" as an analogue to a colour index can be seen as follows: we define an index $m_{\rm L} - m_{\rm C}$ as the difference between a narrow and a broad flux band centred on the line, analogous to the β-index:

$$m_{\rm L} - m_{\rm C} = -1.086 \ln \frac{\sum S_x W_x^{\rm L} / \sum W_x^{\rm L}}{\sum S_x W_x^{\rm C} / \sum W_X^{\rm C}} + \text{constant}. \quad (3)$$

Now, assuming $C_x = C = \sum S_x W_x^{\rm C} / \sum W_x^{\rm C}$ (2) can be rewritten

$$\Lambda^{\rm L} = \sum W_x^{\rm L} - \frac{\sum S_x W_x^{\rm L}}{\sum S_x W_x^{\rm C}} \sum W_x^{\rm C}, \quad (4)$$

which can be inserted in (3), where we get

$$m_{\rm L} - m_{\rm C} = -1.086 \ln \left(1 - \frac{\Lambda^{\rm L}}{\sum W_x^{\rm L}}\right). \quad (5)$$

If we look at variations $\delta(m_{\rm L} - m_{\rm C})$ and $\delta\Lambda$ around the mean values we then get

$$\delta(m_{\rm L} - m_{\rm C}) = 1.086 \frac{\delta\Lambda^{\rm L}}{\sum W_x^{\rm L}(1 - \Lambda^{\rm L} / \sum W_x^{\rm L})} \propto \delta\Lambda^{\rm L}, \quad (6)$$

and we thus see that $\delta(m_{\rm L} - m_{\rm C})$ and $\delta\Lambda$ are directly proportional, showing that the line index can be thought of as a colour index calculated using software filters.

One may of course define any number of line-indices for any spectral line by varying the filter-function used, hereby gaining information from different parts of the line. The choice of filter shape is not critical. We have used a so-called super-Gaussian filter with exponent 8, i.e.:

$$W_x = \exp\left(-\left(\frac{x - x_0}{b}\right)^8\right). \quad (7)$$

The software for calculating line-indices and for performing the time series analysis has been collected in a software package named *Ix*, described by Dall (2000b).

2.2. Mode identification from line-index and photometry

The mode identification proposed here relies on the investigation by Bedding et al. (1996) of the sensitivity of different absorption lines to pulsation modes with different ℓ. For non-rotating stars they showed that the Balmer lines have sensitivity similar to radial velocity measurements because of the strong limb darkening in these lines. Photometry on the other hand has very weak centre-to-limb variation.

Thus photometry and the line-indices of Balmer lines show different response to spatial variations across the stellar disk (i.e. to the ℓ value), because the Balmer lines sample the centre of the disk stronger than the limb while photometry smears out spatial variations across the disk.

Table 1. Sites participating in the spectroscopic campaign. The name abbreviations stand for Nordic Optical Telescope, Thüringer Landessternwarte, Okayama Astrophysical Observatory, Vainu Bappu Observatory, McDonald Observatory. D is telescope aperture diameter in meters, E- means echelle spectrograph in either Cassegrain (Cs) or Coudé (Co) focus.

Name	Location	D	Inst.	R	Observers
NOT	Canary I.	2.54	E-Cs	4300	Dall
TLS	Germany	2.0	E-Co	20000	Lehman
OAO	Japan	1.88	Co	12000	Kambe, Fukata, Nagae
VBO	India	2.3	Cs	130	Anupama
McD	Texas	2.1	E-Co	45000	Handler, Horner

It follows that the ratio R between the amplitudes of the Balmer line-index and the photometry should be an increasing function of ℓ, so that modes with different ℓ should be grouped in an amplitude ratio diagram. This applies only to a slowly rotating star.

Some concern about the ability of the method to discriminate between modes of different spherical degree has been raised by Balona (2000), who used stellar models to investigate the sensitivity of R on ℓ. He finds in addition a strong dependence on $\sin i$ and m. His results will be addressed later. Indeed, for rotating stars the picture becomes much more complicated (Kjeldsen et al. 1998): as rotation increases, gravitational darkening becomes more important. This effect causes a stronger sensitivity to the azimuthal number m, because the orientational degeneracy is lifted. So we get in turn a dependence on the inclination angle. As shown by Hansen (1999) and Frandsen (2000), the m dependence is as least as strong as the ℓ dependence, with the values of amplitude ratios between photometry and line-index varying strongly with $\sin i$. Thus, to disentangle the ℓ and m dependencies, knowledge of the inclination angle is essential, which in turn means that the rotation period and $v \sin i$ must be known independently.

Viskum et al. (1998) conducted a detailed analysis of FG Vir that resulted in a suggestion of mode identification for the 8 strongest modes. This suggestion was later found to agree with an independent mode identification by Breger et al. (1999). In FG Vir a long period variation in the Hα and FeI line-indices, found by Viskum et al. was attributed to stellar activity and thus gave directly the rotation period of the star and, with the observed value of $v \sin i$, also the inclination angle.

3. Observations

The participating observatories (Table 1) represent a large diversity of telescope sizes and of instrumentation both in terms of resolution and efficiency.

Details of the observations conducted at each site are given below. Table 2 gives a log of the observations.

Table 2. Log of the observations. See caption of Table 1 for the abbreviations.

UT Day of Feb. 98	Site	Length (hours)	No. of spectra
3.81	TLS	7.0	60
4.82	TLS	7.7	92
11.74	VBO	3.3	23
11.89	NOT	7.3	105
12.69	OAO	2.0	17
12.72	VBO	2.3	19
13.09	McD	6.7	83
13.42	OAO	6.0	58
13.84	NOT	6.5	57
14.80	TLS	0.8	10
15.25	McD	1.0	18
15.51	OAO	6.8	66
15.84	NOT	8.4	91
16.20	McD	0.3	7
16.56	OAO	4.8	49
16.83	NOT	8.6	101
17.07	McD	1.7	21
17.41	OAO	8.3	78
17.87	NOT	9.3	95
18.06	McD	7.7	91
18.76	TLS	7.0	84
In total:		113.5	1225

Nordic Optical Telescope 7 nights from 11 to 17 February, with the nights of 12th and 14th lost entirely due to bad weather. A total of 449 echelle spectra in 41.5 hours were taken with exposure times between 180 and 300 s, most frequently around 240 s. The spectra were obtained with the ALFOSC instrument, covering 6 partially overlapping orders including Hα and Hβ. Due to the long readout time of the full CCD ($\sim$80 s) the frames were windowed as tightly as possible, with the side effect that the overscan strip information was lost.

The data are of high quality and provide the backbone of the data set.

Thüringer Landessternwarte The 2 meter telescope with echelle spectrograph at Coudé focus observed on the nights of 3, 4, 14, and 18 February for a total of 22.5 hours, giving a total of 246 echelle spectra. Time sampling was 300 s on most nights (420 s on February 3).

Good quality data with a clear oscillation signal in $\Lambda^{\mathrm{H}\alpha}$.

Okayama Astrophysical Observatory 268 spectra were obtained over a total of 28.1 hours. Integration times were about 300 s. The observations ran from 12 to 17 February with the night of the 14th lost to bad weather.

Two different slit widths were used, giving resolutions of 12 500 and 10 200 respectively. The spectra have quite low S/N due to the combination of high resolution and short exposures, but nevertheless the oscillation signature is found to be present in the set.

Vainu Bappu Observatory 10 to 12 February with the 10th being completely cloudy. With a total observing time of 5.4 hours, 42 spectra were obtained with the OMR spectrograph (Prabhu et al. 1998). From this site some two hours were also spent on BV Cnc. Sampling interval was between 300–420 s.

The data are of good quality with a clearly visible oscillation signal in $\Lambda^{\mathrm{H}\alpha}$ despite the short series.

McDonald Observatory 12 to 17 February with plenty of bad weather. When it was possible to observe it happened mostly through clouds with resulting bad S/N. The data consists of high resolution echelle spectra, unfortunately with very low throughput, which further diminished the count rate. Despite of this, the oscillation pattern is recognised in the data.

3.1. Summary of observations

In general all sites collected high quality data despite the poor weather conditions. Especially the large gap between February 4th and 10th is unfortunate, but not critical. Even with spectra of such varying characteristics, the oscillation signal known to be present in BN Cnc is detected in all the individual data sets, although in some cases with very low S/N.

4. Data reduction

The data were reduced by the observers and delivered to T. H. Dall as one dimensional spectra. Different reduction methods have been used as chosen by the observers. Parts of the McDonald data were given a first reduction by Horner, and later completed by Dall.

Nordic Optical Telescope All basic reductions and extraction of one dimensional spectra were done using IRAF tools.

All spectra had bias subtracted after correcting for bad columns on the CCD. The scattered light between orders was removed before normalising the master flatfield. After flat-fielding, the orders were extracted and normalized with the Blaze function of the flatfield.

We chose to normalize the orders with the Blaze function of the flatfield instead of using the Blaze for the individual images, in order to use a constant normalization. This causes the spectral orders to be sloped because of the temperature difference between the flatfield lamp and the star. However, this does not influence the subsequent analysis, as no absolute spectral quantities are sought.

The NOT data did not contain an overscan strip, but this does not appear to be critical. Bias frames were taken at the beginning and end of each night, and no major drifts were found.

The spectra were not continuum normalized and no wavelength calibrations were done. The order containing Hα is shown for a NOT spectrum in Fig. 3.

Thüringer Landessternwarte The reduction was performed using MIDAS. After bias subtraction, correction for bad columns and flat-fielding, the orders were extracted and normalized with a Blaze function fitted to the spectra.

Wavelength calibrations were done using ThAr spectra. The MIDAS wavelength calibration routines were modified to give a better fit at the overlapping edges of the spectral orders.

Finally, all orders were merged into a single one-dimensional spectrum. An example of a spectrum is shown in Fig. 4.

Okayama Astrophysical Observatory All reductions were performed using IRAF. First, bias and dark level were subtracted, before proceeding to flat-fielding with a master flatfield constructed from ten individual exposures.

The spectra were then aperture extracted and wavelength calibrated using Th-Ar spectra. An example of an extracted spectrum is given in Fig. 5.

Vainu Bappu Observatory The various tasks for spectroscopic data reduction under the IRAF package were used for the data reduction.

All spectra were bias subtracted using a mean bias value and flat-field corrected. The spectra were extracted using the optimal extraction method of IRAF. Several Fe-Ne source spectra were obtained during the observations and an average source spectrum weighted according to the times of observation was used for the wavelength calibration.

No flux calibration has been applied. A spectrum can be seen in Fig. 6.

McDonald Observatory All reductions were performed using IRAF tasks. First bias was subtracted, and bad column correction was applied. A master flatfield was constructed for each night and the orders normalized before the flat-fielding. Then the orders were extracted and normalized with the Blaze function of the flatfield (see discussion above for NOT data).

No flux calibrations or wavelength calibrations were performed. An example of one order, containing Hα is given in Fig. 7.

5. Data merging

The only prominent line present in all spectra is Hα, so only this line has had its line-index calculated and used for the subsequent analysis. Due to differences in S/N and resolution the individual sets of spectra are very different. However, the total flux in a spectral line (i.e. the EW) should be independent of resolution.

As mentioned in Sect. 2.1, a given line index will be proportional to the EW of the line, so that for Hα:

$$\Lambda_i^{\mathrm{H}\alpha} = k_i^{\mathrm{H}\alpha} EW(\mathrm{H}\alpha), \tag{8}$$

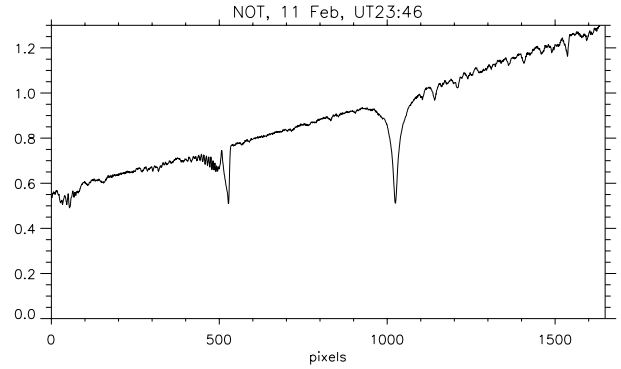

Fig. 3. One order from a spectrum taken from NOT. The red side is to the left. Hα and some atmospheric bands are clearly visible.

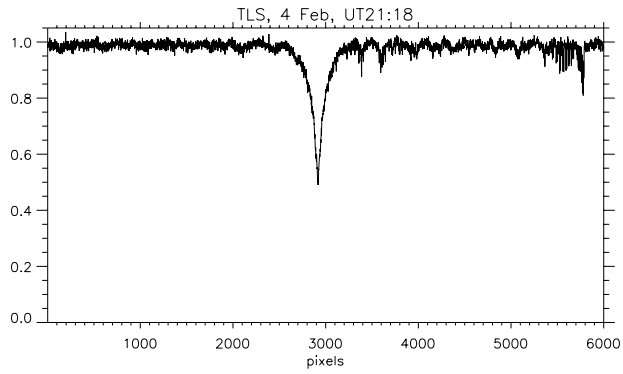

Fig. 4. The combined spectrum from TLS. Red side to the left.

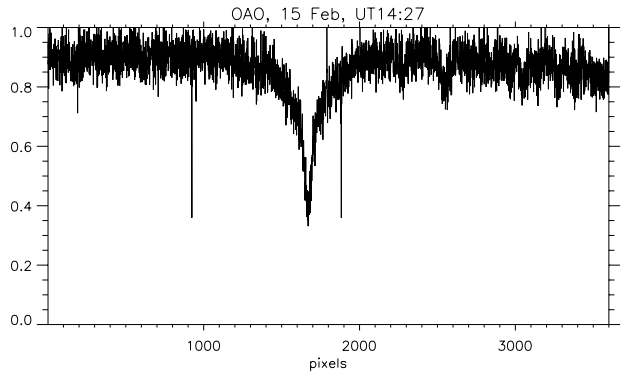

Fig. 5. Spectrum from OAO around Hα line. Relatively high noise because of low count rate in high resolution.

where the index i refers to the choice of filter and the proportionality constant $k_i^{\mathrm{H}\alpha}$ will depend on the FWHM (in wavelength units) of the filter. In order to be able to combine all observations, we had to make sure that the proportionality constant in Eq. (8) was the same for all sets.

The line-index was calculated with a fixed filter width (in pixels) for each individual observatory's data, chosen so that the mean value of the line-index divided by the filter width was the same throughout the full data set. This means that the line-index filter integrates the same part of the line in all data sets regardless of resolution and it ensures that the resulting amplitudes are directly comparable. The filter was indeed found to have approximately the same width in Ångströms for all the individual sets, as expected.

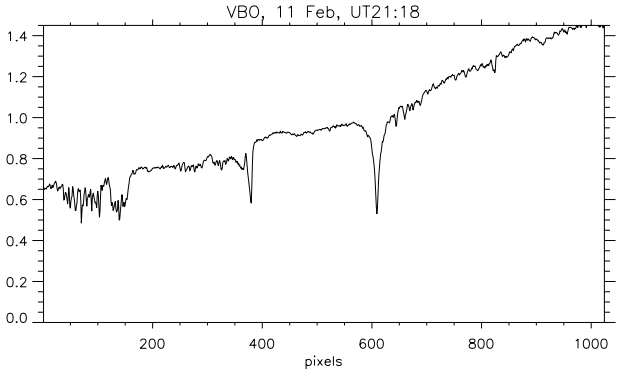

Fig. 6. Spectrum from VBO. Clear Hα and atmospheric bands.

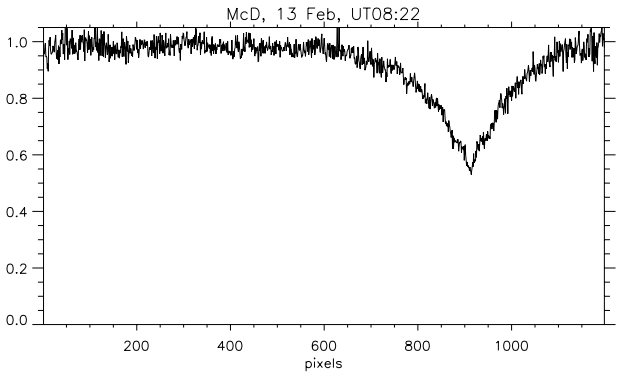

Fig. 7. Spectrum from McD. The order containing Hα. Again low counts due to high resolution. The throughput was measured to be only $\sim$1.7%

The full data set can then be normalized by scaling each subset to a common mean value, which amounts to transforming the individual pixel units of the line-indices to a common unit.

Finally, the scaled data points were assigned statistical weights calculated from the local scatter in the series.

6. Time series analysis

The final series for analysis contains 1225 data points of $\Lambda^{\mathrm{H}\alpha}$ measurements spanning two weeks, but with long periods without observations. The ultimate goal is to derive amplitudes of the modes which are known to be present in BN Cnc, and for which accurate frequencies have been found in the simultaneous STACC 1998 photometric campaign (Paper I). We do not attempt to determine the frequencies from the spectroscopic data set, but use the values from Paper I exclusively.

For this analysis the weighting scheme and sine-wave fitting code described in Frandsen et al. (1996) has been used. The same procedure was used in Paper I. Running the entire data set through this produces the amplitude spectrum of Fig. 8. Note that *promille* is parts-per-thousand, and that 1 promille equals 1.086 mmag.

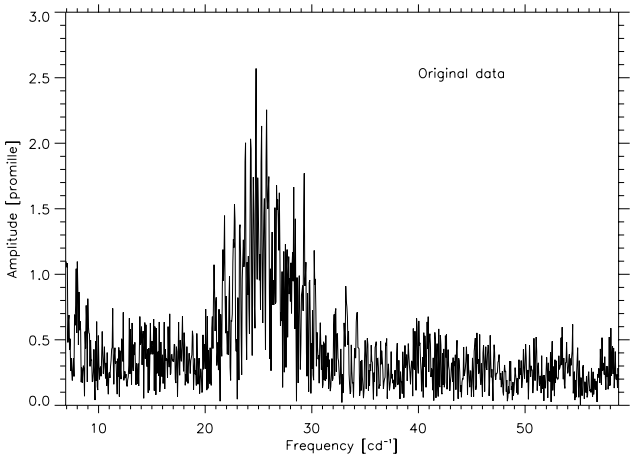

Fig. 8. Amplitude spectrum of the full Hα line-index data set. The oscillation modes are clearly visible, although they are not well resolved.

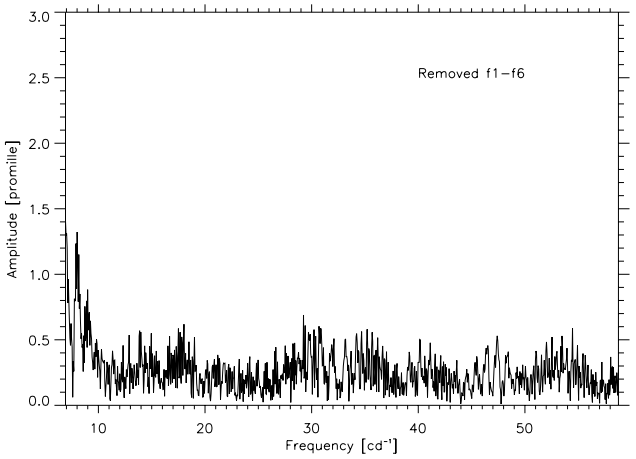

Fig. 9. Amplitude spectrum of the complete data set after pre-whitening with the six frequencies known from Paper I. The noise level is 0.21 promille at high frequencies.

In order to extract the amplitudes of the oscillation modes, an iterative procedure pre-whitening only with the frequencies found in Paper I was performed as follows:

- Initial calculation:
  - first amplitude found and subtracted;
  - second amplitude found and subtracted;
  - ...
  - last amplitude found and subtracted.
- Iterate until convergence:
  - one amplitude recalculated with all other amplitudes subtracted;
  - repeat recalculations until convergence.

The amplitude spectrum after removal of the modes by the above procedure is shown in Fig. 9, and the extracted amplitudes are listed in Table 3. In the cleaned amplitude spectrum there are several bumps left of excess power at a very low level. The highest of these are at or just below 30 cd^{-1}, where also excess power was found in photometry. However, with a $S/N < 4$, we cannot assign frequencies or amplitudes to this, even though there may very well be additional low amplitude modes present.

To construct a reliable amplitude ratio between photometry and line-index, the above procedure was repeated with a time series constructed from the same times as the line-index, but with amplitudes and phases taken from the results of the photometric campaign. This then eliminates any errors that may be introduced by data sampling, and provides an estimate of the errors of the extracted amplitudes. This was repeated with varying amounts of white noise added to the series. For per-point-noise levels below 0.05 promille we recover essentially the input amplitudes by this procedure, with a small error that does not seem to improve as the noise input is decreased. This error is then adopted as the zero-level noise contribution $\sigma_{\rm ex}$ from the extraction procedure, which is orders of magnitude lower than the typical errors on the amplitudes, wherefore we can safely neglect this contribution.

Table 3. Frequencies in cd^{-1} from Paper I and the amplitudes found using the procedure described in the text. The amplitude ratio is $R\alpha = A(\mathrm{H}\alpha)/A(\mathrm{phot})$. $A(\mathrm{H}\alpha)$ are in promille and $A(\mathrm{phot})$ are in mmag.

ν(Paper I) [cd^{-1}]	amplitudes from this work $A(\mathrm{H}\alpha)$	$A(\mathrm{phot})$	$R\alpha$
$f_1 = 25.7611$	2.34 ± 0.20	2.99 ± 0.08	0.78 ± 0.09
$f_2 = 23.0298$	1.28 ± 0.18	2.53 ± 0.08	0.51 ± 0.14
$f_3 = 28.2704$	1.69 ± 0.26	2.41 ± 0.08	0.70 ± 0.16
$f_4 = 22.7835$	1.84 ± 0.19	2.26 ± 0.09	0.81 ± 0.11
$f_5 = 25.9396$	1.00 ± 0.21	2.14 ± 0.09	0.46 ± 0.21
$f_6 = 25.4367$	1.29 ± 0.20	0.62 ± 0.08	2.09 ± 0.20

The noise at high frequencies in the Hα line-index is 0.21 promille, corresponding to a per-point-noise of ∼4 promille, which is much higher than the error from the pre-whitening procedure. The errors on $A(\mathrm{H}\alpha)$ are then found from the residual amplitude spectrum, by averaging the remaining signal around each frequency. The same procedure was used in Paper I.

The amplitudes and the amplitude ratios for the six frequencies are given in Table 3 and Fig. 10 shows the amplitude ratios as a function of frequency.

7. Discussion

We will concentrate on two main aspects in the following: the technical and observational one as well as the scientific outcome.

7.1. What is new?

In the so-called Aarhus-diagram of Viskum et al. (1997, 1998) the amplitude ratios of $\Lambda^{\mathrm{H}\alpha}$ and $\Lambda^{\mathrm{H}\beta}$ relative to the photometric amplitude are plotted against each other. From the grouping of the modes in this diagram (ideally along a straight line $R_\alpha = R_\beta$) the degree of the mode can then be found: low values would correspond to low degree modes and higher values to higher degree modes, that is

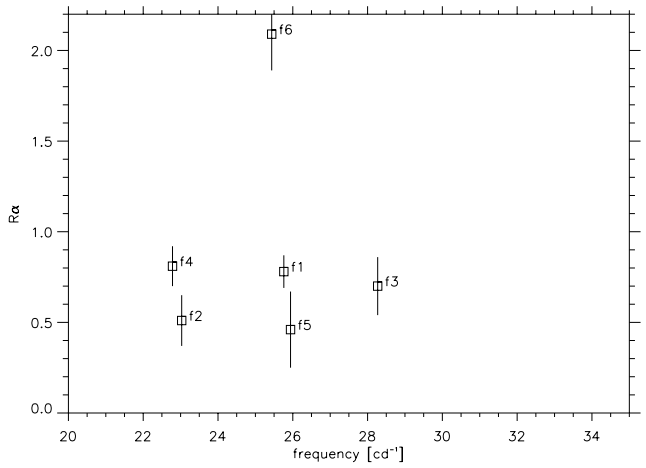

Fig. 10. The amplitude ratios shown as function of frequency.

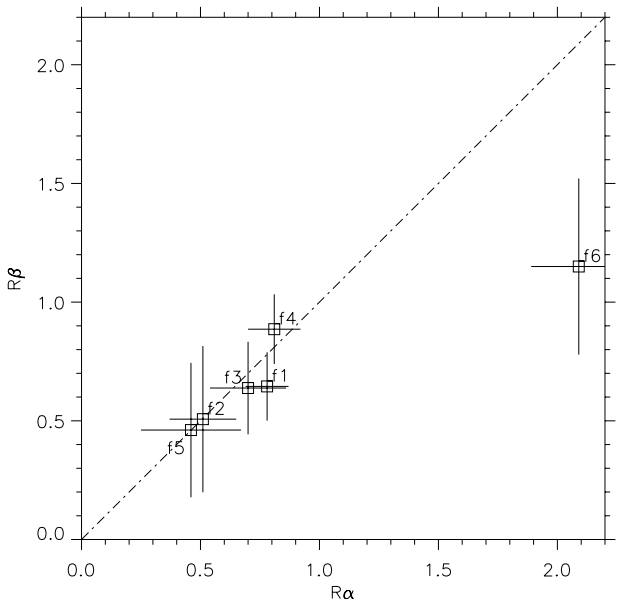

Fig. 11. Amplitude ratios of Hα and Hβ relative to photometry. The dashed line show $R\alpha = R\beta$. Generally there is good agreement between the two ratios, despite the higher noise in Hβ.

modes with more spatial variation across the stellar disk. This easy interpretation is only valid for a slow rotator, where the azimuthal parameter m only weakly affect the R_α observable.

For a moderately to fast rotating star this straightforward interpretation is altered, as the modes group according to both ℓ and m for these stars, and for fast rotators the dominant role may be played by m in connection with the inclination angle. The reason is that gravity darkening becomes as important as limb darkening.

In the case of BN Cnc we can expect the m dependence to be at least as significant as the ℓ dependence for the amplitude ratio of a given mode. As a consequence the R_α observable only provides an indicator of the degree of surface structure of the observed modes. It can still be used to divide the observed modes in certain classes, containing only a subset of the total modes.

A sensible approach to Fig. 10 is to identify the two modes f_2 and f_5 as modes with small spatial structure. If there are radial modes among the observed set, these two modes are thus prime candidates. This can be concluded without reference to any other evidence. It actually turns out to be consistent with the results of Hernández et al. (1998) that there can be at most two radial modes in this star. They found a small set of solutions that were within the uncertainty of the parameters for the cluster and the star, taking rotation into account. Earlier, ignoring rotation, the f_5 and f_4 modes were assigned $n = 6$ and $5, \ell = 0$ by Perez Hernandez et al. (1995). The analysis, including effects of rotation, is not able to discriminate against any of the choices (f_2, f_5) and (f_4, f_5) as sets of radial modes. Even (f_2, f_1) is an acceptable pair giving a frequency ratio within the possible parameter space.

The f_6 mode would need to have high spatial structure, meaning that it cannot be radial and most likely can be assigned to $\ell = 2, m = 0, \pm 2$, since according to Frandsen (2000) only such a mode can achieve such high values of R. Higher ℓ values are not likely, as the mode is observed photometrically.

Table 4. The identifications from this work and comparison with previous suggestions. Amplitudes are given in promille for $\Lambda^{\mathrm{H}\alpha}$ and in mmag for the photometry of Paper I.

mode	Amplitude from		Mode ID	
	$\Lambda^{\mathrm{H}\alpha}$	Paper I	this work	previous[a]
f_1	2.34	3.01	$\ell = 1$	
f_2	1.28	2.52	$n = 5, \ell = 0$	
f_3	1.69	2.42	$\ell = 1$	
f_4	1.84	2.32	$\ell = 1$	$n = 5, \ell = 0$
f_5	1.00	2.13	$n = 6, \ell = 0$	$n = 6, \ell = 0$
f_6	1.29	0.63	$\ell = 2 - 3$	

[a] Perez Hernandez et al. 1995, but see text.

As a check, using only the NOT data, R_β was found and confirmed the low ratio of the f_2 and f_5 modes, and the high ratio of the f_6 mode, see Fig. 11.

The remaining modes are difficult to classify. If one accepts that f_2 and f_5 are radial, then they have to be non-radial modes. If we assume that f_2 corresponds to $n = 5$ and f_5 to $n = 6$, it is possible that f_4, f_1, and f_3 are $\ell = 1$ belonging to consecutive orders, e.g. $n = 5, 6, 7$. Additional observations are needed to sort this out.

In Table 4 we summarise the mode information, and the proposed identifications.

In the previous studies of BN Cnc (and other variables in Praesepe), a search for the correct frequency ratios based on model predictions has been used to select possible pairs of radial modes. Arentoft et al. (1998) calculated the frequencies for two radial orders for an evolutionary sequence of models and approximated these with analytical relations given in their Eq. (2).

For a given choice of radial modes, the luminosity L will be a function of the effective temperature T_{eff}. We

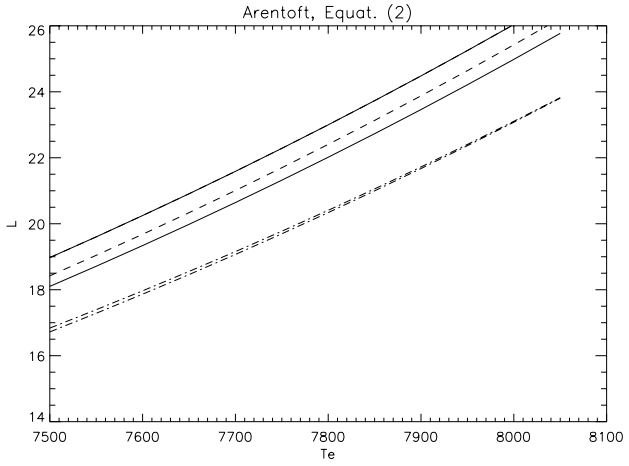

Fig. 12. Luminosity–temperature relations for the Arentoft et al. models selecting radial modes $f(n = 5)$ and $f(n = 6)$. The dot-dashed lines show the relations for the (wrong) identification presented in that paper, while the upper lines are based on the present identification (full) and the Perez Hernández et al. identification (dashed).

present in Fig. 12 the $L-T_{\rm eff}$ relations for the choice of the radial modes $f(n = 5)$ and $f(n = 6)$ found in the present paper, as well as from Hernández et al. (1998) and from Arentoft et al. (1998). The solution, which brings the two curves closest (dot – dashed), is in our opinion incorrect. It has however precisely the right frequency ratio according to the models applied, which do not include rotation. It leads to an underestimate of the luminosity if the temperature is known. In addition the identification is based on a mode, which is not present in our time series.

Hernández et al. came very close to our proposed solution. They have had a difficult case due to the presence of close frequencies of modes with similar amplitudes. The effect is minor and using non-rotating models the luminosity found from the mode identification in this paper and Hernández et al. is the same: $L/L_{\odot} = 22$ for $T_{\rm eff} = 7750$ K.

It is clear that using frequency ratios as the criteria only gives a hint to what might be radial modes. The same can be said about the evidence coming from observations of R_{α} and R_{β}. However, if the two criteria agree for a mode, the probability of the identification being correct is considerably increased.

One of the reasons that frequency ratios are not such reliable indicators is the large value of the rotational velocity $v \sin i$ in BN Cnc and other Praesepe variables. They all have values above 100 km s^{-1} except KW 284. The modeling is difficult and rotation also affects radial modes due to second or higher order terms. For BN Cnc, calculations by Kjeldsen et al. (1998) give changes for $n = 5$ and $n = 6$ of the order 1 μHz. At the same time the frequency ratio $f(n = 6)/f(n = 5)$ changes from 1.1434 for a non-rotating star to 1.1386 for the rotating star. The change in effective temperature with the inclination angle ($\sin i$) amounts to 100 K and the change of the apparent luminosity can be up to 10%. As $\sin i$ can not be measured, there are plenty of models that fit in the available parameter space.

Using the amplitude ratios R presented in this paper eliminates a lot of this freedom and points to the radial modes as those with small R values.

Is there any theoretical support for the conclusions about mode types in BN Cnc? Balona (2000) has performed extensive calculations of the *EW* variations for a small set of stellar models with parameters corresponding to δ Scuti stars. Simpler calculations for the ratio R have been carried out by Hansen (1999) summarized by Frandsen (2000, Eq. (9)). *In the first calculation* a stellar disk integrated line profile is computed at each point in time and the *EW* found by integrating the line profile. Having the detailed shape of the line profile makes it possible to compute other observables like line profile moments. Complete account of the Doppler shifts is secured. *The second calculation* derives the change in flux and the change of the *EW* for each surface element and then calculates the average for the whole stellar disk. Doppler shifts do not enter in this case. One can describe this as filter calculations.

The way the results obtained by Balona (2000, Figs. 1–3) are displayed makes the comparison with observations and other calculations difficult. All unstable modes are included in the diagrams regardless of the amplitude. Thus modes, which will have very small photometric amplitude occur although they in practice are unobservable photometrically.

The calculations by Hansen (1999) show the expected dependence on the azimuthal number m. The modes with low values R_{α} are found to be $\ell = 0$ or $m = 0$ modes. Depending on inclination higher degree modes can sometimes show odd amplitudes in photometry or *EW* due to strong cancellation during the surface integral and therefore one can sometimes see large variations of the R_{α} parameter.

The difference between the two approaches is in principle only the order in which the integrals are performed. There are a few additional assumptions in the filter calculations, which we do not expect to have any major influence on the main results.

The results from the detailed line profile studies by Balona (2000) and the filter calculation by Hansen (1999) and Frandsen (2000) should be compared in detail; the filter calculations are relatively easy and fast to perform and in most cases sufficient for the interpretation of the *EW* results, but a verification is needed.

The R values for radial modes should, according to the filter calculations we have performed, be quite similar. This is consistent with the results from Fig. 10 and with the values observed for FG Vir (Viskum et al. 1998), where $R \sim 0.5$ and for ρ Pup (Dall et al., unpublished), where $R \sim 0.43$. The observations do not show the spread in R seen in Figs. 1–3 in Balona (2000), but this might be due to the inclusion of the more extended range of modes in Balona's figure.

More studies of the usefulness of the observations of amplitude ratios are needed. These ratios do seem to provide an additional source of information, not necessarily

Table 5. Phase differences between the oscillations of $\Lambda_{\mathrm{H}\alpha}$ and photometry.

mode	$\phi_{\Lambda(\mathrm{H}\alpha)} - \phi_{\mathrm{phot}}$ [degrees]
f_1	55 ± 5
f_2	136 ± 8
f_3	-8 ± 9
f_4	-10 ± 6
f_5	31 ± 12
f_6	100 ± 12

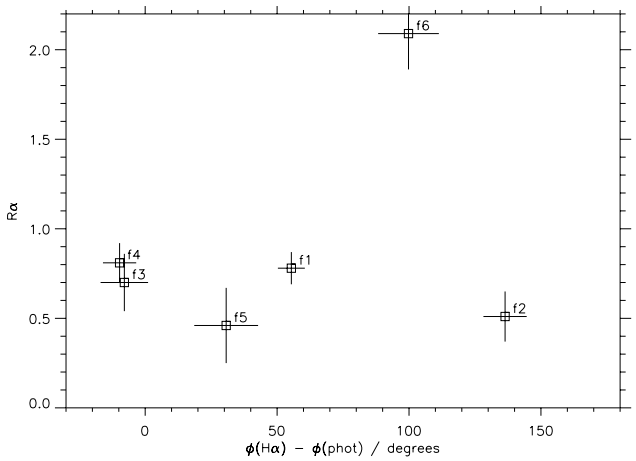

Fig. 13. Amplitude ratios as function of phase differences. The phases are given in degrees.

superior to other diagnostics, but providing independent confirmation of the type of the modes. For a slow rotator like FG Vir the R_α parameter has been shown to be an indicator of the ℓ value. For BN Cnc it can be used to identify candidates for radial modes, but the interpretation is more complicated and other observables, like line profile moments, are needed to complete an identification.

We have also investigated the phase differences between the oscillations in $\Lambda^{\mathrm{H}\alpha}$ and photometry. They are listed in Table 5, and shown in Fig. 13. We show R_α as a function of the phase difference. This resembles the well known photometric mode discrimination diagram (e.g. Garrido 2000), where an amplitude ratio between a colour index and a photometric band is plotted as a function of their phase differences. The grouping of modes in such a diagram can then, if one has a good model, help to identify the modes.

Recently Paparo & Sterken (2000) discussed the mode-typing potential of a wide selection of amplitude ratios and phase differences in the Strömgren photometric system. Based on an empirical approach they identified some promising discriminators, $A(b)/A(y)$ and $\phi_{b-y} - \phi_b$, without trying to explain the physical reasons for the observed groupings of modes. With our Fig. 13 we could take a similar approach and try to identify a pattern based on the already suggested radial modes f_2 and f_5. Note that the range in phase difference here is much larger than any observed between photometric bands.

Unfortunately, we do not have calculations, that permit us to make any interpretation of the phase differences. Let it be sufficient to note that it provides additional information about the modes, yet waiting to be understood.

7.2. Spectroscopic requirements

This campaign has brought together very different instrumentation in an effort to get as good temporal coverage as possible. The temporal coverage has not been as good as suggested by the distribution of sites, which can mainly be attributed to bad weather at all sites, plus the fact that some sites got only short allocations of time.

The diversity of the instrumentation has proved problematic. While oscillation signatures were found in all data sets, the noise was in many cases very high. There can be several causes for this: telescope tracking/guiding inaccuracy which likely worsens in bad weather conditions, instrumental instabilities or data reduction noise.

However, a very basic limitation is of course simple photon statistics: it was required to keep exposure plus readout times below ∼500 s to get sufficient sampling. For some combinations of telescope, spectrograph and detector, this requirement means that the resulting S/N is quite low, and the weighting of these data is correspondingly low. In particular the data from OAO and McD suffered from this problem, which is disappointing as these sites are situated at key longitudes. Recently the instrumentation at OAO was updated causing an overall increase in efficiency.

Instrumental instabilities Movements of the spectral lines due to spectrograph flexure is critical if one is not very careful with the flatfielding or if the CCD has variable sensitivity. This will of course mainly be a problem for Cassegrain instruments.

At the NOT such movements can amount to several pixels during a night, while at VBO the maximum shift from the beginning of the observations to the end is only around 0.5 pixels making drift problems insignificant. Since we do not see indications of instabilities in the NOT data we conclude that instrumental drifts are unlikely to be significant sources of errors.

8. Conclusions

We have demonstrated that the simultaneous photometry provides us with a very firm foundation: we have used the frequency solution found from photometry to limit the number of free parameters and thus we have obtained very accurate oscillation amplitudes in $\Lambda^{\mathrm{H}\alpha}$. This allows us to directly compare with the photometric amplitudes and to establish reliable amplitude ratios, that reflect the

geometry of the mode and hence enable us to characterize the modes.

BN Cnc is the first case of a rapidly rotating δ Scuti star where we have been able to identify with some certainty the nature of the modes. Two modes have low values of the R_α ratio and are candidates for radial modes. They turn out to have the right frequency ratio for the mass and distance derived earlier by Hernandez et al. (1998). Three modes pose as low order non-radial modes, probably $\ell = 1$, because there are only two radial modes in the frequency range and $\ell = 2$ or higher degrees normally come out with low photometric amplitudes. Finally, the last mode is of higher degree, probably $\ell = 2$ as it is detected photometrically with an amplitude 3–4 times lower than the other modes we see. The suggested identifications need verification by other methods as in the case of FG Vir, where the two methods applied agree in 7 out of 8 cases.

We find indications of undetected modes, both in photometry and spectroscopy. These may well be high order modes, since their signatures are slightly more visible at the higher noise levels of the spectroscopy.

The constraints on the duty cycle proved to be severe for sites with smaller telescopes or low instrument efficiency which caused a degradation of S/N. For the planning of future campaigns it is very important to consider this in great detail to ascertain that the time allocated is used in the most efficient way.

Acknowledgements. Nordic Optical Telescope is operated on the island of La Palma jointly by Denmark, Finland, Iceland, Norway, and Sweden, in the Spanish Observatorio del Roque de los Muchachos of the Instituto de Astrofisica de Canarias.

The data presented here have been taken using ALFOSC, which is owned by the Instituto de Astrofisica de Andalucia (IAA) and operated at the Nordic Optical Telescope under agreement between IAA and the NBIfAFG of the Astronomical Observatory of Copenhagen

THD acknowledges support from the Danish Space Board under the Danish Ministery of Research, J.nr. 456-9601878.

GH's observations were partially supported by the Austrian Fonds zur Förderung der Wissenschaftlichen Forschung under grant S7304.

References

Aerts, C., & Eyer, L. 2000, in Delta Scuti and Related Stars, ed. M. Breger, & M. H. Montgomery, ASP Conf. Ser., 210, 113

Arentoft, T., Kjeldsen, H., Nuspl, J., et al. 1998, A&A, 338, 909

Baldry, I. K., Bedding, T. R., Viskum, M., Kjeldsen, H., & Frandsen, S. 1998, MNRAS, 295, 33

Baldry, I. K., Viskum, M., Bedding, T. R., Kjeldsen, H., & Frandsen, S. 1999, MNRAS, 302, 381

Balona, L. A. 2000, MNRAS, 319, 606

Bedding, T. R., Kjeldsen, H., Reetz, J., & Barbuy, B. 1996, MNRAS, 280, 1155

Breger, M., Pamyatnykh, A. A., Pikall, H., & Garrido, R. 1999, A&A, 341, 151

Dall, T. H. 2000a, in The impact of Large-Scale Surveys on Pulsating Star Research, ed. L. Szabados, & D. W. Kurtz, ASP Conf. Ser., 203, 471

Dall, T. H. 2000b, in The NOT in the 2000s, Conf. Proc.

Dall, T. H. 1998, in The First MONS Workshop: Science with a Small Space Telescope, ed. H. Kjeldsen, & T. R. Bedding (Aarhus University), 115

Frandsen, S., Balona, L. A., Viskum, M., et al. 1996, A&A, 308, 132

Frandsen, S. 2000, in Delta Scuti and Related Stars, ed. M. Breger, & M. H. Montgomery, ASP Conf. Ser., 210, 428

Frandsen, S., Pigulski, A., Nuspl, J., et al. 2001, A&A, 376, 175

Frandsen, S., Pigulski, A., and the STACC team, 2000, in The impact of Large-Scale Surveys on Pulsating Star Research, ed. L. Szabados, & D. W. Kurtz, ASP Conf. Ser., 203, 473

Garrido, R. 2000, in Delta Scuti and Related Stars, ed. M. Breger, & M. H. Montgomery, ASP Conf. Ser., 210, 67

Hansen, E. J. 1999, Masters Thesis (in Danish), Aarhus University

Hernandez, M. M., Perez Hernandez, F., Michel, E., et al. 1998, A&A, 338, 511

Kjeldsen, H., Arentoft, T., Bedding, T. R., et al. 1998, in Stucture and dynamics of the interior of the Sun and Sun-like stars; Proc. SOHO 6/GONG 98 Workshop, ed. S. G. Korzennik, & A. Wilson (ESA SP-418, ESA Publications Division)

Mantegazza, L., in Delta Scuti and Related Stars, ed. M. Breger, & M. H. Montgomery, ASP Conf. Ser., 210, 138

O'Toole, S., Teixeira, T. C., Bedding, T. R., & Kjeldsen, H. 2000, in The impact of Large-Scale Surveys on Pulsating Star Research, ed. L. Szabados, & D. W. Kurtz, ASP Conf. Ser., 203, 519

Pamyatnykh, A. A., Dziembowski, W. A., Handler, G., & Pikall, H. 1998, A&A, 333, 141

Paparo, M., & Sterken, C. 2000, A&A, 362, 245

Perez Hernandez, F., Claret, A., & Belmonte, J. A. 1995, A&A, 295, 113

Prabhu, T. P., Anupama, G. C., & Surendiratnath, R. 1998, Bull. Astron. Soc. India, 26, 383

Rodríguez, E., López-González, M. J., & López de Coca, P. 2000, A&AS, 144, 469

Schrijvers, C., Telting, J. H., Aerts, C., et al. 1997, A&AS, 121, 343

Sperl, M., 1998, Comm. Asteroseismology (Vienna), 111, 1

Telting, J. H., & Schrijvers, C. 1997, A&A, 317, 723

Viskum, M., Kjeldsen, H., Bedding, T. R., et al. 1998, A&A, 335, 549

Viskum, M., Dall, T. H., Bruntt, H., et al. 1987, in A Half Century of Stellar Pulsation Interpretation, A Tribute to Arthur N. Cox, ed. P. A. Bradley, & J. A. Guzik, ASP Conf. Ser., 135, 465